Hindawi
Advances in Civil Engineering
Volume 2022, Article ID 2812413, 7 pages
https://doi.org/10.1155/2022/2812413

Research Article

Experimental Study on Gas Permeability Semiempirical Model of Granite after Heat Treatment

Jinquan Wu [1,2]

[1]*Key Laboratory of Geological Survey and Evaluation of Ministry Education, China University of Geosciences (Wuhan), Wuhan 430074, China*
[2]*Lincang Transportation Bureau of Yunnan Province, Lincang 677099, China*

Correspondence should be addressed to Jinquan Wu; 951426185@qq.com

Received 7 May 2022; Accepted 18 August 2022; Published 6 September 2022

Academic Editor: Wei-yao Guo

High temperature will cause a thermal crack of a rock, thus affecting the permeability change of rock. To explore the effects of temperature on permeability and microstructure of rock microstructure, the granite after 50–800 C thermal treatment was carried out by gas permeability test, combined with computed tomography (CT) scanning technology. The granite internal three-dimensional reconstruction was conducted after high-temperature thermal treatment, and the characteristics of the microstructure were also deeply analyzed. On this basis, the applicability of the Costa model under high temperature was discussed. Finally, the temperature-permeability model of granite after the high temperature was proposed combined with the pore fractal model. The new model was verified with experimental data.

1. Introduction

In recent years, with the rapid development of nuclear power, the output of nuclear waste has been increasing year by year. At present, the international common way of disposal is through the construction of underground nuclear waste repository thousands of meters underground and the use of geological barriers and artificial barriers to permanently block the nuclide movement. In the process of geological storage of nuclear waste, nuclides release heat energy, which leads to the increase of surrounding rock temperature. These fractures are interconnected and act as pathways for nuclides to migrate to the biosphere. Therefore, it is a key scientific problem to study the effect of high-temperature heat treatment on the evolution of microstructure and seepage characteristics of low permeability rocks [1–5].

In term of describing the fractal characteristics of the internal microstructure of rock after thermal fracture, some research used the method of the scanning electron microscope (SEM) or optical microscope to carry out 2D geometric analysis of the images of rock surface [6–9]. The result cannot effectively reflect the 3D characteristics of the real rock's internal microstructure. For porous media, mercury intrusion porosimetry (MIP) is an effective tool to obtain the pore size distribution [10]. The basic step is to obtain the volume of mercury intrusion under different pressures by mercury injection experiments and then calculate the pore size distribution by the cumulative mercury injection volume [11–13]. In recent years, as a method that can directly reflect the three-dimensional microstructure of rock, computed tomography (CT) has been more applied [14, 15]. CT technology is characterized by no-contact, accurate, and fast. Yu et al. [16] reconstructed the digital 3D model of jointed sandstone with CT technology and applied the digital model to simulate the uniaxial compression process.

As for establishing the relationship between the permeability and the microscopic characteristics of rocks, most of the applicable permeability models are semiempirical ones due to the great discreteness and complexity of the microstructure. The K-C model, which is based on the Poiseuille equation (17), has been widely accepted by scholars. On the basis of the K-C model, many modified models have been proposed. Table 1 summarizes the main

Table 1: K-C model and its main modified model.

Scholars	Model	Definition of parameters
Kozeny [18], Carman [19]	$k = C_{kc}\varphi^3/(1-\varphi)^2$	$C_{kc} = c/8\tau^2 s_0^2$
Rodriguez [20], Shih [21]	$k = C_{kc}\varphi^{n+1}/(1-\varphi)^n$	
Bayles [22]	$k = C_b\varphi^{2+n}/(1-\varphi)^2$	$C_b = c/8bs_0^2$
Costa [23]	$k = C_c\varphi^n/1-\varphi$	$C_c = cA_{l\mu}/b$

Figure 1: Rock specimen.

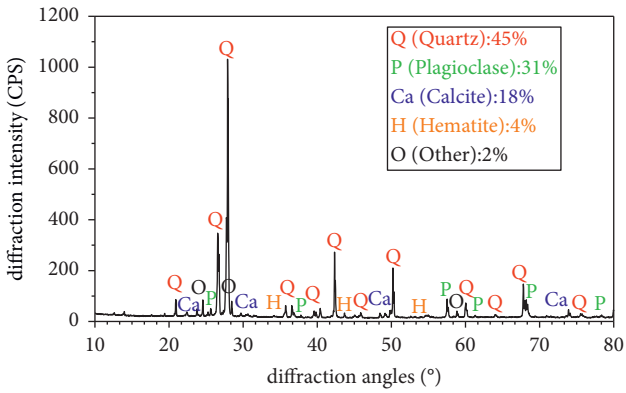

Figure 2: X-ray diffraction pattern of granite.

modified models and gives the definition of the empirical parameters. Although the permeability model, which reflects the relationship between macroscopic permeability and microscopic characteristics of rock, has become mature, there are few reports on the models of the variation of rock permeability with temperature after thermal treatment. Therefore, the purpose of this work is to establish the temperature-dependent permeability model of granite after high-temperature heating treatment.

(c is the geometrical equivalent factor, τ is tortuosity, s_0 is the specific surface area of particles, n is the cementation factor of Archie's equation, b is the tortuosity factor of Archie's equation, $A_{l\mu}$ is the sum of the total area of pores with diameters less than the $l\mu$).

2. Rock Specimen Preparation and Experiment

2.1. Rock Specimen Preparation. To reduce the heterogeneous of granite specimens, the granite was cored in a rock block from Hunan Province, China, at the depth of 50 ~ 70m underground. The specimen is drilled with a laboratory rig and made into cylindrical specimens with a diameter of 50 mm and a height of 100 mm for the gas permeability tests, as shown in Figure 1. Also, the upper and lower ends of the granite specimen were polished with sandpaper to ensure the degree of parallelism and verticality are less than 0.02 mm. The X-ray diffraction pattern of the granite is shown in Figure 2. The result shows that the specimens are made of quartz, plagioclase, calcite, hematite, and a small amount of other minerals.

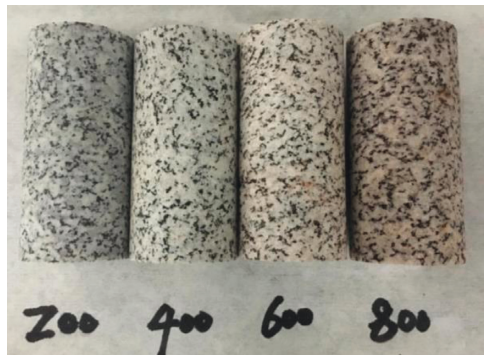

Figure 3: Granite specimens after high-temperature heating treatment.

2.2. Thermal Treatment. The heat treatment was carried out in the Rock Mechanics Laboratory of Wuhan University. The rock specimen is heated by a box-type furnace SX21012 made by Yahua Company. The heating step can be preset according to requirement, and it has a maximum heating temperature 1100 °C and a corresponding maximum error ±1.0°C. The furnace chamber with a size of 250 mm × 400 mm × 160 mm is sufficiently large to heat 10 specimens simultaneously.

Twenty-five granite specimens were divided into five groups, and a group includes five granite specimens. The specimens were heated to 50 °C, 200°C, 400°C, 600°C, and 800°C at a rate of 10°C/min. The temperature rises linearly to a specified value and then remains constant for 10 hours. The specimens were then naturally cooled to room temperature at a cooling rate of 10°C/min and kept at room temperature for 24 hours before gas permeability tests were performed. Figure 3 shows granite specimens after heat treatment at different temperatures. As the temperature increases from 50°C to 800°C, the color of the rock specimen changes from bluish-gray to white.

2.3. Gas Permeability Test. The transient pulse decay method is widely used to measure gas permeability in low permeability materials, such as rock. The gas permeability of

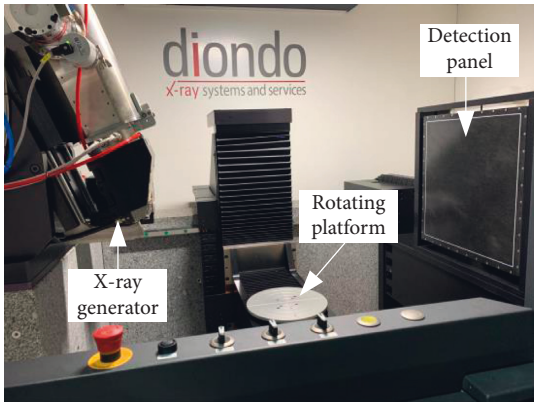

Figure 4: CT detection system.

granite at different temperatures was measured by a hydro-mechanical coupling system, autonomous designed by the Institute of rock and soil mechanics, and the Chinese academy of sciences. All tests are conducted at constant temperature (20°C).

First, the confining pressure of the chamber is maintained at 2.5 MPa. Nitrogen was inserted to maintain a pressure of 0.9 MPa in the upper chamber. The specimen was kept saturated in the triaxial cell of gas injection, and the gas injection was balanced at the lower chamber increasing to 0.9 MPa. Subsequently, the chamber pressure was increased to 6.95 MPa, and the effective confining pressure was maintained at 6.0 MPa. Finally, pulse attenuation tests were carried out under a hydrostatic state, and an injection 0.1 MPa brings the upper reservoir pressure to 1.0 MPa. In the process of tests, the upper and lower pressures are self-recorded by the computer every 5 seconds. Before tests, each specimen must be stored in an oven and dried at 50°C for at least three days.

Liu et al. [24] derived the expression of gas permeability in the transient-flow test. During pulse decay tests, the relation between the upper and lower differential pressure ΔP_0 at the beginning of the experiment and the upper and lower differential pressure $\Delta P(t)$ after time t of the experiment can be described as follows:

$$\frac{\Delta P(t)}{\Delta P_0} = e^{-st},$$
$$s = \frac{Ak}{L\mu z}\left(\frac{1}{V_{up}} + \frac{1}{V_{dn}}\right), \quad (1)$$

where k is the gas permeability of the material, L, A are the length and cross-sectional area of the specimen, μ and z are the dynamic viscosity and the critical compressibility of the gas, which value is 1.80×10^{-5} Pa·s and 0.292 $mm^2 \cdot °C^{-1}$, respectively, for nitrogen. V_{up} and V_{dn} are the volumes of upper and lower reservoirs, respectively. The gas permeability can be calculated by equation (1) and equation (2) using gas pressure data

3. Rock Microstructure Representation

3.1. CT Scanning. Internal microstructure of granite was obtained by a Diondo d2 high-resolution CT detection system, manufactured by German Diondogmbh, which had a spatial resolution of 20 μm. The CT detection system (Figure 4) comprises an X-ray beam, a detector panel, and a rotating platform. The X-ray beam penetrating the specimen is measured by an array of detectors. The X-ray is produced by electrons striking a Mo–W alloy target in an X-ray tube. The electron current is 80 lA, the accelerating voltage is 140 kV, and the scanning time is 4 s. The degree of X-ray attenuation depends on the density and the atomic numbers of the materials in the specimens (Savaş and Marva [25]).

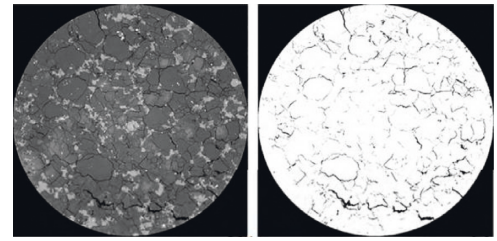

Figure 5: Cross-sectional gray CT image.

Prescanning must be carried out before CT measurements. First, the granite specimen is placed on the rotating platform. Then, the granite specimen is prescanned, and the position of it is fine-tuned according to the receiving result of the detector panel. At the beginning of the measurement, the rotating platform rotates at a constant speed, and the computer collects data every fixed time. The X-ray attenuation matrix is obtained by X-ray scanning in different directions, and then, the gray-scale cross-sectional images of the granite specimen are obtained.

In order to ensure the measurement precision, the magnification is 200, and the minimum observable scale is 25 mm. Figure 5 shows a cross-sectional gray scale image result (256-order gray scale used in the study) obtained from this X-ray micro-CT scanning. It can be seen that the surface crack is clearly observed. This indicates that, in this study, X-ray micro-CT scanning has a high-resolution ability to obtain internal crack in granite material.

According to Lambert's law [9], the gray scale reflects the density of the mineral. So, the distribution of porous and various mineral components in granite can be identified by the gray scale.

3.2. 3D Micropore Structure Reconstruction Method. The internal pore or fracture in granite is a flow path, which determines its permeability. So, it is necessary to further process the obtained CT cross-sectional image to extract the pores or fractures. A method distinguishing rock matrix and rock fracture or pore was developed by Xiong et al. [26]. Figure 6 shows the fracture or pore results using this method, the fracture or pore microstructure in the granite is shown in black (Gray value = 0), and the granite matrix is shown in white (gray value = 1).

The digital image consists of a rectangular array of pixels. Each pixel is the region at the intersection of any horizontal and vertical scan lines, all of which are of equal width h. Therefore, each pixel can be considered a square element. The material structure captured in the cross-sectional CT

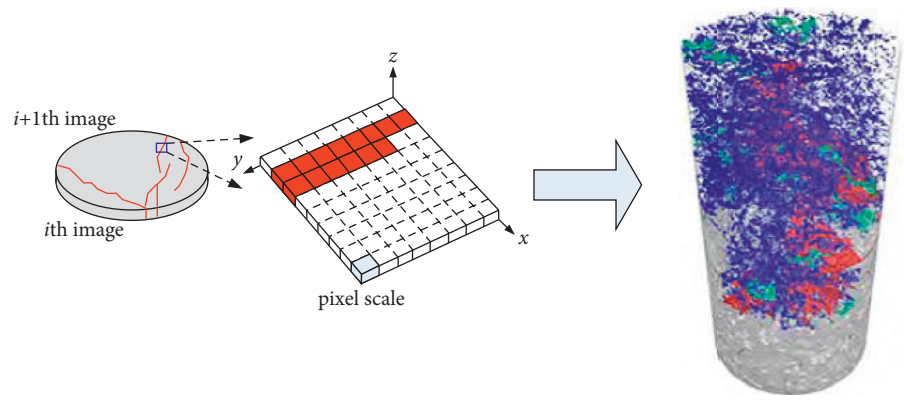

Figure 6: Schematic of three-dimensional reconstruction process of rock.

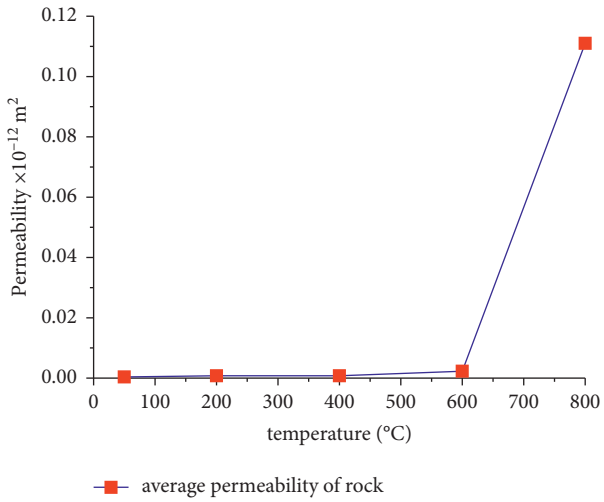

Figure 7: The influence of heating temperature on permeability.

image is assumed as that of a layer with a d height. Based on this, the granite microstructure represented by the image can be easily mapped to a layer of the cuboid grid of the same size, which is generated by a rectangular array of image pixels extending vertically. Figure 6 shows the generated 3D microstructure model.

4. Experiment Results

4.1. Permeability of Granite. The permeability of the granite after thermal treatment at different temperatures is shown in Figure 7. As shown in Figure 7, when the temperature is lower than 400°C, the permeability of granite changes a little. The temperature increases from 50 to 400°C, and permeability only increases from $3.8e-16$ to $7.6e-16\,m^2$. When the heating temperature is higher than 400 °C, the permeability of granite increases exponentially. The permeability of granite for 800°C is 146 times higher than that of 400°C. It is indicating that temperature has a significant impact on permeability when heating temperature greater than 400 °C.

4.2. 3D Micropore Structure Analysis. A three-dimensional reconstruction method was used to obtain the internal microstructure geometry structure of granites at different temperatures, as shown in Figure 8. As can be seen from Figure 8, when the temperature is lower than 400 °C, the pores generated by thermal loading in granite are mostly microporous. When the temperature exceeds 400 °C, the number of pores increases. When the temperature reaches to 800°C, the fracture going through the granite appears. It is predicted that the number of fractures increases as temperature increases. Figure 9 shows the volume proportion of microstructure in different volume intervals inside granite after thermal treatment at different temperatures. In terms of the proportion of microstructure in different volume intervals, when the temperature is lower than 400°C, the volume of microstructure in granite is mainly distributed in the range of 0.001-0.1 mm^3, the distribution curve of the volume proportion is similar, and the peak value is around 0.01 mm^3. When the thermal treatment temperature rises to 600 °C, the peak value of the volume distribution of the internal microstructure of granite moves to the right range of 0.1-1 mm^3, and the maximum thermal fracture pore volume is significantly increased compared with 400°C, which is located near 10 mm^3. When the temperature reaches to 800 °C, the peak value of the internal microstructure of granite appears at the right end, and the pore volume distribution in other sections is more even. The main reason for this situation is that the internal fractures develop rapidly under high temperature, and most of the isolated pores wrapped by minerals with poor thermal stability are connected with each other, thus forming large volume fractures. Finally, the pore distribution in each volume interval is relatively smooth, and the volume proportion of large volume connected fractures appears to the peak.

5. Temperature-Permeability Model and Its Verification

The Kozeny and Carman model (K–C model) and Costa model [27, 28] derived from the capillary bundle model are generally used to describe the permeability of porous and low-permeability rocks, which are expressed as

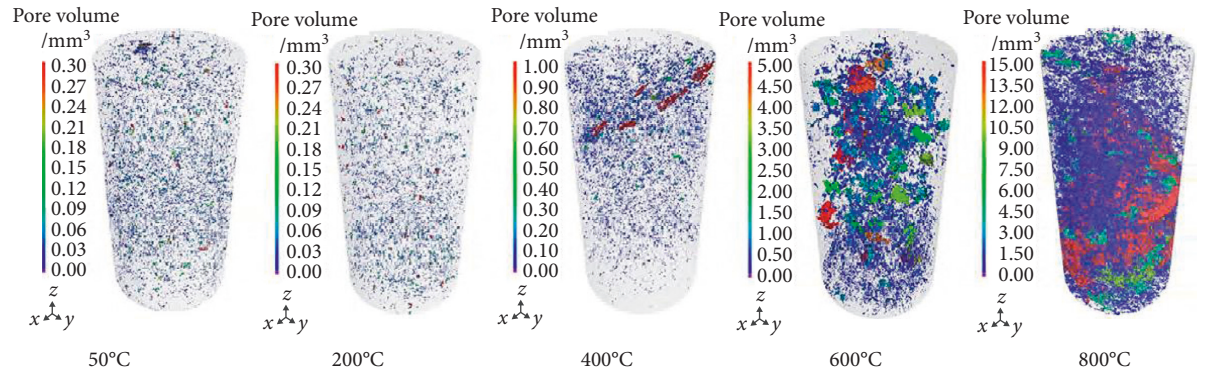

Figure 8: Rendering model of microfracture after thermal treatment at different temperatures.

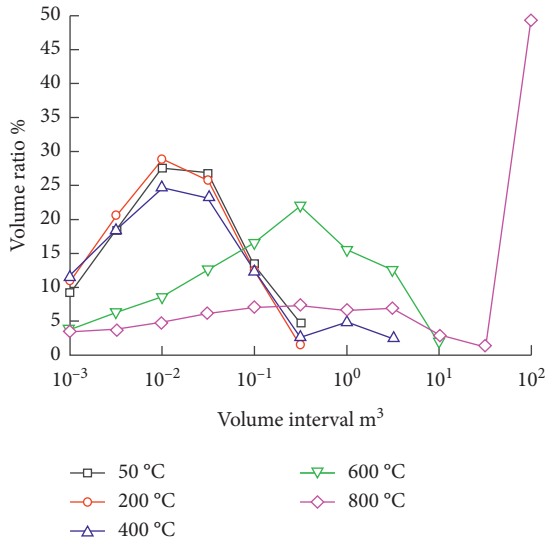

Figure 9: Proportion of microstructures in each volume interval of granite.

$$k = C_{K\text{-}C}\frac{\phi^3}{(1-\phi)^2},$$
$$k = C_C\frac{\phi^n}{1-\phi}, \tag{2}$$

where $C_{K\text{-}C}$ and C_C are K–C coefficient and Costa coefficient, respectively. It is proved that the Costa model is more applicable for high pore rock [29, 30]. The pore in granite is assumed as Sierpinski shim and Menger sponge, and a fractal model of pore volume representing rock geometry can be obtained as

$$V(\geq r) = V_a\left[1-\left(\frac{r}{L_2}\right)^{3-D}\right], \tag{3}$$

where $V(\geq r)$ is the pore volume whose pore size is greater than or equal to r. This parameter can be considered as CT scanning accuracy. V_a is the total volume of rock within the scale range L_2, and D is the fractal dimension. Hence, the pore of rock ϕ is expressed as

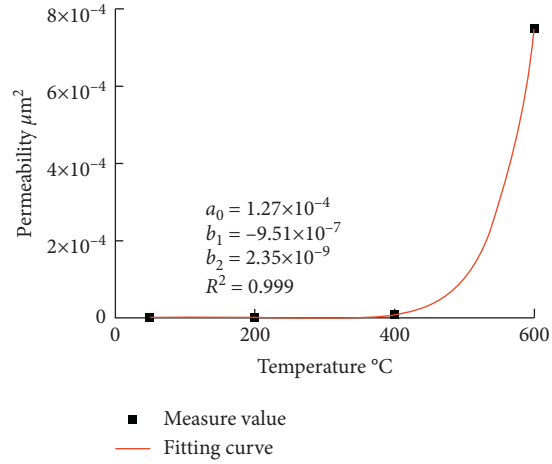

Figure 10: Fitting results of the temperature-permeability model.

$$\phi(\geq r) = \frac{V(\geq r)}{V_a} = 1-\left(\frac{r}{L_2}\right)^{3-D}. \tag{4}$$

Substituting (4) into equation (4), a permeability model of granite under high temperature can be obtained as

$$k = C_C\left(\frac{L_2}{r}\right)^{3-D}\left[1-\left(\frac{r}{L_2}\right)^{3-D}\right]^n. \tag{5}$$

Zhang et al. [31] studied the effects of thermal treatment temperature 25–1200 °C on fractal structure characteristics of granite, and their study demonstrates that the relationship between the fractal dimension D of granite and temperature T could be expressed as

$$D = a + b_1T + b_2T^2. \tag{6}$$

Hence, a temperature-dependent permeability model can be obtained as

$$k = C_C\left(\frac{L_2}{r}\right)^{a_0+b_1T+b_2T^2}\left[1-\left(\frac{r}{L_2}\right)^{a_0+b_1T+b_2T^2}\right]^n. \tag{7}$$

The permeability data of granite after a high temperature of 50–600°C are used to fit (7). Figure 10 shows the relationship between permeability and temperature of granite.

As can be seen in Figure 10, fitting results show that the fitting degree of the new model is above 0.99, so the proposed model can be used to predict the permeability of granite after high temperature treatment. This proposed model has an important engineering significance. For example, the relationship between temperature and permeability of rock should be mastered in betweengeological storage of nuclear waste. Furthermore, the temperature-dependent permeability model of rock extends understanding of high-temperature rock mechanics.

6. Conclusion

The gas seepage tests and CT scanning of granite after different temperatures treatment were conducted to systematically study its evolution mechanism of the internal microstructure and permeability. A new semiempirical permeability model is proposed and verified by the experimental results, and the main conclusions are as follows:

(1) Gas permeability test shows that the permeability of granite changes a little when the temperature of thermal treatment is lower than 400°C and increases exponentially when the temperature is greater than 400°C.

(2) When the temperature is less than 400°C, the pores generated by thermal loading in granite are mostly microporous. When the temperature exceeds 400°C, the number of pores increases. When the temperature reaches 800°C, the fracture going through the granite appears.

(3) Based on the Costa model, the granite temperature-dependent permeability model is deduced. The new model reflects the relationship between the temperature of thermal treatment and the permeability of granite. Finally, the new proposed permeability is verified by the gas permeability test results. The result shows that the proposed model has high accuracy to predict the gas permeability of granite after thermal treatment at different temperatures.

Data Availability

The data that support the findings of this study are available from the corresponding author upon reasonable request

Conflicts of Interest

The authors declare that they have no conflicts of interest.

Acknowledgments

This work was supported by the National Natural Science Foundation of China (Grant no. 42077243).

References

[1] Z. C. Tang, Z. L. Wu, and J. Zou, "Appraisal of the number of asperity peaks, their radii and heights for three-dimensional rock fracture," *International Journal of Rock Mechanics and Mining Sciences*, vol. 153, Article ID 105080, 2022.

[2] Z. Tang and M. Sun, "Mechanical properties of marble with varying slenderness ratios after high temperatures," *International Journal of Geomechanics*, vol. 22, no. 7, Article ID 04022088, 2022.

[3] Z. C. Tang, Q. Z. Zhang, and J. Peng, "Effect of thermal treatment on the basic friction angle of rock joint," *Rock Mechanics and Rock Engineering*, vol. 53, no. 4, pp. 1973–1990, 2020.

[4] Y. Y. Jiao, K. Wu, J. Zou et al., "On the strong earthquakes induced by deep coal mining under thick strata-a case study," *Geomechanics and Geophysics for Geo-Energy and Geo-Resources*, vol. 7, no. 4, p. 97, 2021.

[5] S. Esmaeili, H. Sarma, T. Harding, and B. Maini, "Review of the effect of temperature on oil-water relative permeability in porous rocks of oil reservoirs," *Fuel*, vol. 237, pp. 91–116, 2019.

[6] Z. C. Tang, M. H. Peng, and S. Xiao, "Basic friction angle of granite fracture after heating and rapid cooling treatments," *Engineering Geology*, vol. 302, Article ID 106626, 2022.

[7] C. C. Xia, Z. C. Tang, W. M. Xiao, and Y. L. Song, "New peak shear strength criterion of rock joints based on quantified surface description," *Description Rock Mechanics and Rock Engineering*, vol. 47, no. 2, pp. 387–400, 2014.

[8] D. Xue, H. Zhou, Y. Zhao, L. Zhang, L. Deng, and X. Wang, "Real-time SEM observation of mesoscale failures under thermal-mechanical coupling sequences in granite," *International Journal of Rock Mechanics and Mining Sciences*, vol. 112, pp. 35–46, 2018.

[9] Q. Zhe, H. Fu, and X. Chen, "A study on altered granite meso-damage mechanisms due to water invasion-water loss cycles," *Environmental Earth Sciences*, vol. 78, no. 14, pp. 1–10, 2019.

[10] F. Zhao, Q. Sun, and W. Zhang, "Fractal analysis of pore structure of granite after variable thermal cycles," *Environmental Earth Sciences*, vol. 78, no. 24, pp. 677–691, 2019.

[11] E. W. Washburn, "The dynamics of capillary flow," *Physical Review*, vol. 17, no. 3, pp. 273–283, 1921.

[12] W. Friesen and R. Mikula, "Fractal dimensions of coal particles," *Journal of Colloid and Interface Science*, vol. 120, no. 1, pp. 263–271, 1987.

[13] H. Ranaivomanana, A. Razakamanantsoa, and O. Amiri, "Permeability prediction of soils including degree of compaction and microstructure," *International Journal of Geomechanics*, vol. 17, no. 4, Article ID 04016107, 2017.

[14] H. Ni, J. Liu, B. Huang et al., "Quantitative analysis of pore structure and permeability characteristics of sandstone using SEM and CT images," *Journal of Natural Gas Science and Engineering*, vol. 88, Article ID 103861, 2021.

[15] R. Lopes and N. Betrouni, "Fractal and multifractal analysis: a review," *Medical Image Analysis*, vol. 13, no. 4, pp. 634–649, 2009.

[16] Q. Yu, S. Yang, P. G. Ranjith, W. Zhu, and T. Yang, "Numerical modeling of jointed rock under compressive loading using X-ray computerized tomography," *Rock Mechanics and Rock Engineering*, vol. 49, no. 3, pp. 877–891, 2016.

[17] N. A. Mortensen, F. Okkels, and H. Bruus, "Reexamination of Hagen-Poiseuille flow: shape dependence of the hydraulic resistance in microchannels," *Physical Review*, vol. 71, no. 5, Article ID 057301, 2005.

[18] J. Kozeny, "Ueber kapillare Leitung des Wassers im Boden," *Stizungsber. Akad Wiss Wien*, vol. 136, pp. 271–306, 1927.

[19] P. Carman, "Fluid flow through granular beds," *Transactions of the Institution of Chemical Engineers*, vol. 15, pp. 150–167, 1973.

[20] E. Rodriguez, F. Giacomelli, and A. Vazquez, "Permeability-porosity relationship in RTM for different fiberglass and natural reinforcements," *Journal of Composite Materials*, vol. 38, no. 3, pp. 259–268, 2004.

[21] C. H. Shih and L. J. Lee, "Effect of fiber architecture on permeability in liquid composite molding," *Polymer Composites*, vol. 19, no. 5, pp. 626–639, 1998.

[22] G. A. Bayles, G. E. Klinzing, and S. H. Chiang, "Fractal mathematics applied to flow in porous systems," *Particle & Particle Systems Characterization*, vol. 6, no. 1-4, pp. 168–175, 1989.

[23] A. Costa, "Permeability-porosity relationship: a reexamination of the Kozeny-Carman equation based on a fractal pore-space geometry assumption," *Geophysical Research Letters*, vol. 33, no. 2, Article ID L02318, 2006.

[24] Z. Liu, J. Shao, S. Xie, and J. Secq, "Gas permeability evolution of clayey rocks in process of compressive creep test," *Materials Letters*, vol. 139, pp. 422–425, 2015.

[25] S. Erdem and M. A. Blankson, "Fractal–fracture analysis and characterization of impact-fractured surfaces in different types of concrete using digital image analysis and 3D nanomap laser profilometery," *Construction and Building Materials*, vol. 40, pp. 70–76, 2013.

[26] F. Xiong, Q. Jiang, and C. Xu, "Fast equivalent Micro-scale pipe network representation of rock fractures obtained by computed tomography for fluid flow simulations," *Rock Mechanics and Rock Engineering*, vol. 54, no. 2, pp. 937–953, 2020.

[27] F. Normant and C. Tricot, "Method for evaluating the fractal dimension of curves using convex hulls," *Physical Review*, vol. 43, no. 12, pp. 6518–6525, 1991.

[28] D. A. Russell, J. D. Hanson, and E. Ott, "Dimension of strange attractors," *Physical Review Letters*, vol. 45, no. 14, pp. 1175–1178, 1980.

[29] J. Hearst, P. Nelson, and F. Pailet, *Well Logging for Physical Properties*, McGraw-Hill, New York, 2000.

[30] G. Archie, "The electrical resistivity log as an aid in determining some reservoir characteristics," *Transaction of American Institute of Mining, Metallurgical, and Petroleum Engineers*, vol. 146, no. 1, pp. 54–62, 1942.

[31] Z. Zhang, F. Gao, Y. Gao, and X. Xu, "Fractal structure and model of pore size distribution of granite under high temperatures," *Chinese Journal of Rock Mechanics and Engineering*, vol. 35, no. 12, pp. 2426–2438, 2016.